Experimental Investigation of the Morphology Development of Polyblends in Corotating Twin-Screw Extruders

H. POTENTE,[1] M. BASTIAN,[1] A. GEHRING,[1] M. STEPHAN,[2] P. PÖTSCHKE[2]

[1] Institut für Kunststofftechnik (KTP), Universität Paderborn, 33095 Paderborn, Germany

[2] Institut für Polymerforschung (IPF), 01069 Dresden, Germany

Received 8 March 1999; revised 25 June 1999; accepted 5 September 1999

ABSTRACT: Compounding extruders are still designed based on experience and time-consuming experimental examinations. This work investigates the morphology development of incompatible polyblends along a mixing zone at the end of a corotating twin-screw extruder. During the process, the samples are taken from the running extruder using special barrel plates. These samples are subsequently examined by means of scanning electron microscopy (SEM). This method allows sampling in less than 1 min and thus extremely fast and almost unaffected. The experimental investigation of the morphology development improves the knowledge about the factors essentially influencing the blending process. It also allows the verification as well as improvement of theoretical models. Polyblends of polypropylene (PP) and polyamide (PA) with 7.5, 15, and 30 wt % PA were examined. As well as the relevance of the mass percentage of the dispersed phase, the influence of the screw geometry, the screw speed, the melt temperature, the melt throughput, and the pressure profile was investigated. Apart from the melt throughput, all varied factors show an influence on the resulting blend morphology that may not be neglected. However, the changes of the mean particle sizes in the observed mixing zones are only gradual (mean particle size $\approx$ 1–4 μm), which can be attributed to the extremely fine blend morphology already existing during or after the melting. That means that the application of "classic melting zones" generally already produces finely dispersed blend morphologies, thus proving the essential importance of the melting zones regarding the development of the blend morphology. Consequently, the mean particle sizes, calculated by means of quantitative image analyses of SEM micrographs in the mixing zones following the homogenizing section only slightly depend on the compounding conditions (screw speed, melt throughput, screw geometry, melt temperature, and pressure profile). However, the direct visual analysis of the SEM images, especially in the first parts of the mixing zones, shows the simultaneous existence of large PA6 particles in the PP matrix. In addition, a downstream unification of the particle size distribution can be observed. Especially the number and size of the coarser particles decreases in the mixing zones. © 2000 John Wiley & Sons, Inc. J Appl Polym Sci 76: 708–721, 2000

Key words: polyblend; morphology; twin screw extruder

INTRODUCTION

Commercial polyblends consist of at least two polymeric components. They allow the combination of favorable properties of known polymers (synergism) as well as the development of new quality characteristics.[1] In general, the development of a new polyblend is also far more cost-effective than that of a new polymer.[2]

During the processing of polyblends and depending on material combination and process control, the mostly single-phase starting materi-

Correspondence to: M. Bastian.

Journal of Applied Polymer Science, Vol. 76, 708–721 (2000)

als form different microstructures inside the solid (morphologies). The deliberate optimization of the material characteristics and consequently of the functional properties by means of the blending process is closely related to the creation of suitable phase morphologies. In order to allow the prediction of the resulting blend morphology by means of process simulations, e.g., with the SIGMA (Paderborn, Germany) simulation software[3–7] exact knowledge of the microrheologic phenomena such as deformation, breakup, and coalescence is necessary. However, for the blend production, the formation of the dispersion and thus the particle size distribution presents a dynamic process, which is determined by the equilibrium of the processes of particle breakup and coalescence of the dispersed phase, taking place in parallel inside the screw compounders.[8] Important for the developing blend structure are mainly the rheologic characteristics of the components (viscosity, elastic characteristics) as well as the system's interfacial tension behavior.[9]

Apart from the materials' influence, the barrel and screw configurations as well as the processing parameters, such as the screw speed, determine the resulting phase morphology and thus the product characteristics. These dependencies are experimentally examined for the melt section in a mixing zone located at the end of the extruder in this work.

It is to be considered that the substantial reduction of the particle size can be observed in that zone of the extruder, where both components are either already completely molten[10] or are in the process of being molten and are thus at least partially present in the form of melt.[11–16] The first drastic reduction of the domains size of the dispersed phase usually only takes a few screw elements, i.e., just a few seconds.[10,11] However, the final morphology, determining the characteristics of the end product, is largely determined by the design of the geometry and the selection of the process conditions and consequently by the flow conditions in the last section of the extruder as well as in the following die.[17–19] Furthermore, the mechanical characteristics of polyblends can largely vary, even if the mean particle size and particle size distribution only slightly changes.[20–22]

EXPERIMENTAL

A binary polymer combination was used, which is completely incompatible, with isolated embedded particles of the dispersed phase in a surrounding matrix. It is the objective of these experiments to investigate the mechanism of the morphology development in melt-filled zones of the twin-screw extruder thus to determine the major influencing factors and also to provide a sufficient database for a comparison of the morphology development with theoretical models[23,24] and their calculated results. This background largely determines the experimental design.

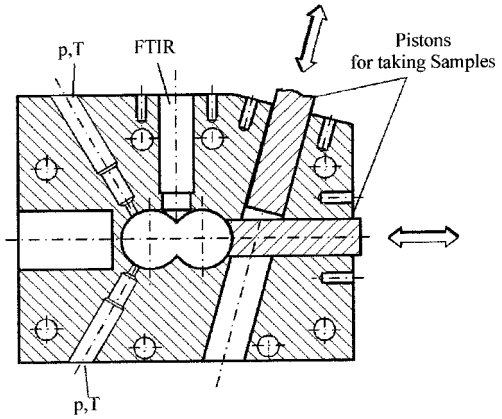

Figure 1 Sample plates (SP)/DE95, Fra97, Fra98/, FTIR, Fourier transform infrared. p = pressure; T = temperature

During the experiments, the geometry of the screw was kept constant between two sampling points, where the morphology was determined. Another aim was to provide as similar processing profiles in these zones as possible, e.g., constant amounts of material and uniform pressure gradients.

The extruder experiments were carried out using a corotating twin-screw extruder made by Krupp Werner and Pfleiderer (KW&P) (Stuttgart, Germany), type ZSK40, fitted with special sample plates (Fig. 1).

These sample plates are parts of the extruder barrel and allow sampling at their point of installation during the ongoing process.[25,26,19] Essentially, a lateral horizontal piston on the sample plate provides access to the screw channel, through which material can flow from the screw channel into a chamber. If the melt pressure is sufficient, the material is automatically fed, or, in case of a degree of filling below 100% it can be pushed out of the sample plate by means of a second piston. This technology allows online sampling at very short sampling times. For the purpose of measuring the crucial processing parameters during the process, each sample plate is equipped with a pressure and a temperature sen-

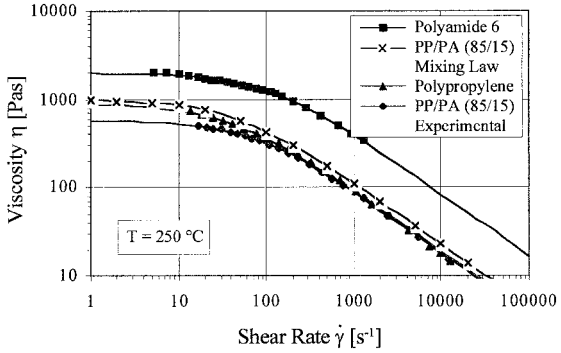

Figure 2 Viscosity curves.

sor, allowing the recording of the real pressure and temperature values during the sampling.

Test Material

A mixture of polypropylene (PP) (Hostalen PPT 1070, Hostalen Polyolefine GMBH, Frankfurt, Germany) and polyamide (PA) 6 (Ultramid B4, BASF AG, Ludwigshafen, Germany) was used as the blend system. This system is incompatible, i.e., thermodynamically not miscible without interfacial reactions. The blend with two clearly separated phases is easy to produce and easy to morphologically examine. Another reason for selecting this material combination is the use of existing test results to be found in literature,[19] which allows a comparison. The PA6 content in the blend is between 7.5 and 30 wt %, so that the PA constitutes the dispersed phase, embedded by the PP matrix.

Rheologic Characteristics

The viscosity curves of the pure material as well as of the blends with 15 wt % PA, measured with the high-pressure capillary rheometer and adjusted with the Carreau equation are shown in Figure 2 for a temperature $T = 250°C$.

The calculated blend viscosity was determined by means of the mixing rule according to Arrhenius[27,28]:

$$\log\eta_{\text{Mix}} = w_c \cdot \log\eta_c + w_d \cdot \log\eta_d. \qquad (1)$$

The viscosity curve of the polymer blend shows that the experimental blend viscosity is lower than the viscosity of the individual components. Therefore, a calculation of the blend viscosity by means of a linear mixing rule such as the statement by Arrhenius is unsuitable for this blend system. This confirms observations made by Han et al.,[29] Plochocki,[30] and Potente et al.,[31] who in experiments with other polymer combinations also determined that simple mixing rules can only inadequately calculate the actual blend viscosity. Therefore, the measured material characteristics of the mixture are used to calculate the process behavior of the twin-screw extruder with SIGMA.[3]

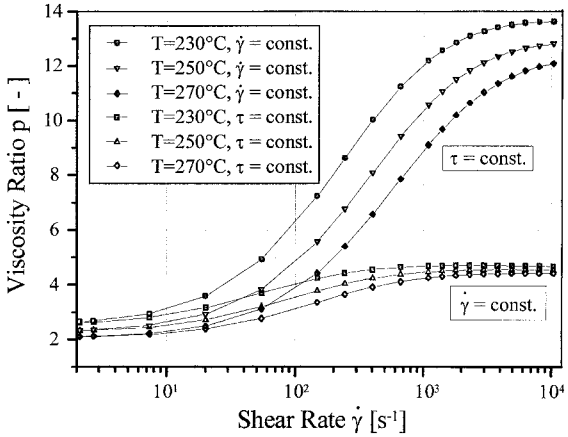

Figure 3 Viscosity ratios between PA6 (as dispersed phase) and PP (as matrix).

Figure 3 shows the viscosity ratio:

$$p = \frac{\eta_d}{\eta_c} \qquad (2)$$

of the two blend components for different temperatures T, for one at a constant shear rate $\dot{\gamma}$ and secondly at a constant shear stress τ.

Figure 3 shows that the way of calculating the viscosity ratio decisively influences this value. For the current PP/PA blend, the viscosity ratio values calculated at the same shear stress are up to 4 times higher than the viscosity ratio values calculated at the same shear rate. Within the extruder's shear rate range of interest of approx-

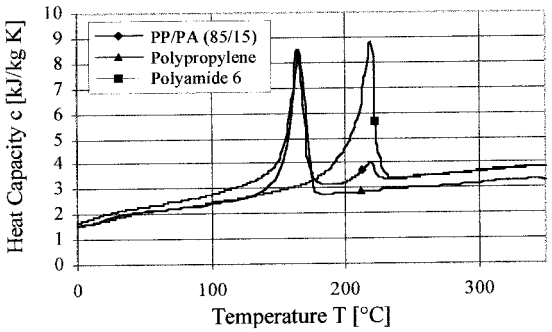

Figure 4 Specific heat capacity versus temperature.

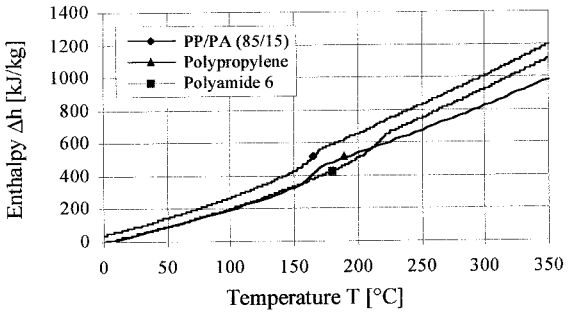

Figure 5 Enthalpy versus temperature.

imately 10 to 1000 s^{-1}, and the achieved processing temperatures, Figure 3 shows viscosity ratios at τ = constant of approximately $2.5 < p < 12$, which although no longer ideal for a good particle breakup, still allow particle size reduction in case of elongation flow.

Thermodynamic Characteristics

The enthalpies and specific heat capacities of the materials, necessary for the SIGMA calculations to predict the process behavior, were determined by means of differential scanning calorimetry (DSC). Figures 4 and 5 show the results of the investigations.

Interfacial Tension

Franzheim has carried out breaking thread experiments for this system and has measured an interfacial tension of $\gamma_{1,2}$ = 9.5 mN/m at a temperature of T = 260°C.[19]

Table I contains all the material data used to calculate the process behavior by means of the SIGMA simulation software.

Screw and Barrel Configurations

Experiments were performed with four different screw configurations (S1 to S4 in Fig. 6) and with four sample plates each, thus providing five sampling points including the die outlet.

The four screw configurations only differ in the zones, in which samples can be taken. Using the four sample plates and including the die provides four screw sections, for which a morphology change can be determined. The measuring sections represent feed zones and kneading zones, with a chosen constant geometry between two points of sampling. The screw element types selected for the measuring zones are conveying kneading blocks with different kneading disc widths and conveying elements with different pitches as well as a re-conveying element, thus

Table I Material Data for a SIGMA Simulation

Material	PP	PA	PP/PA (85/15)
a [Pas]	1069.56	2034.57	576.28
b [s]	0.06337	0.01349	0.01343
c [−]	0.57266	0.59719	0.69536
T_R [°C]	250	250	250
T_S [°C]	154.90	158.92	192.96
C_1 [−]	8.86	8.86	8.86
C_2 [°C]	101.6	101.6	101.6
T_K [°C]	167.30	220.37	219.47
c_0 [kJ/kg K]	2.07057	2.30876	2.30708
c_m [kJ/kg K °C]	0.00368	0.00440	0.00452
Δh_F [kJ/kg]	345.93	463.12	562.89
Δh_A [kJ/kg]	142.26	266.44	246.64
λ_0 [W/mK]	0.11433	0.11617	0.12847
λ_m [W/mK°C]	0.00019	0.00057	0.00028
λ_F [W/mK]	0.167	0.269	0.215
ρ_F [g/cm^3]	0.8996	1.142	0.9201
ρ_S [g/cm^3]	0.50333	0.63	0.4650
v_0 [cm^3/g]	1.12849	0.85798	1.0879
v_m [cm^3/g°C]	0.00098	0.00063	0.00093
$\gamma_{12,0}$ [mN/m]	—	—	12.1
$\gamma_{12,m}$ [mN/m°C]	—	—	0.01
d_G [mm]	3.79	2.76	3.78

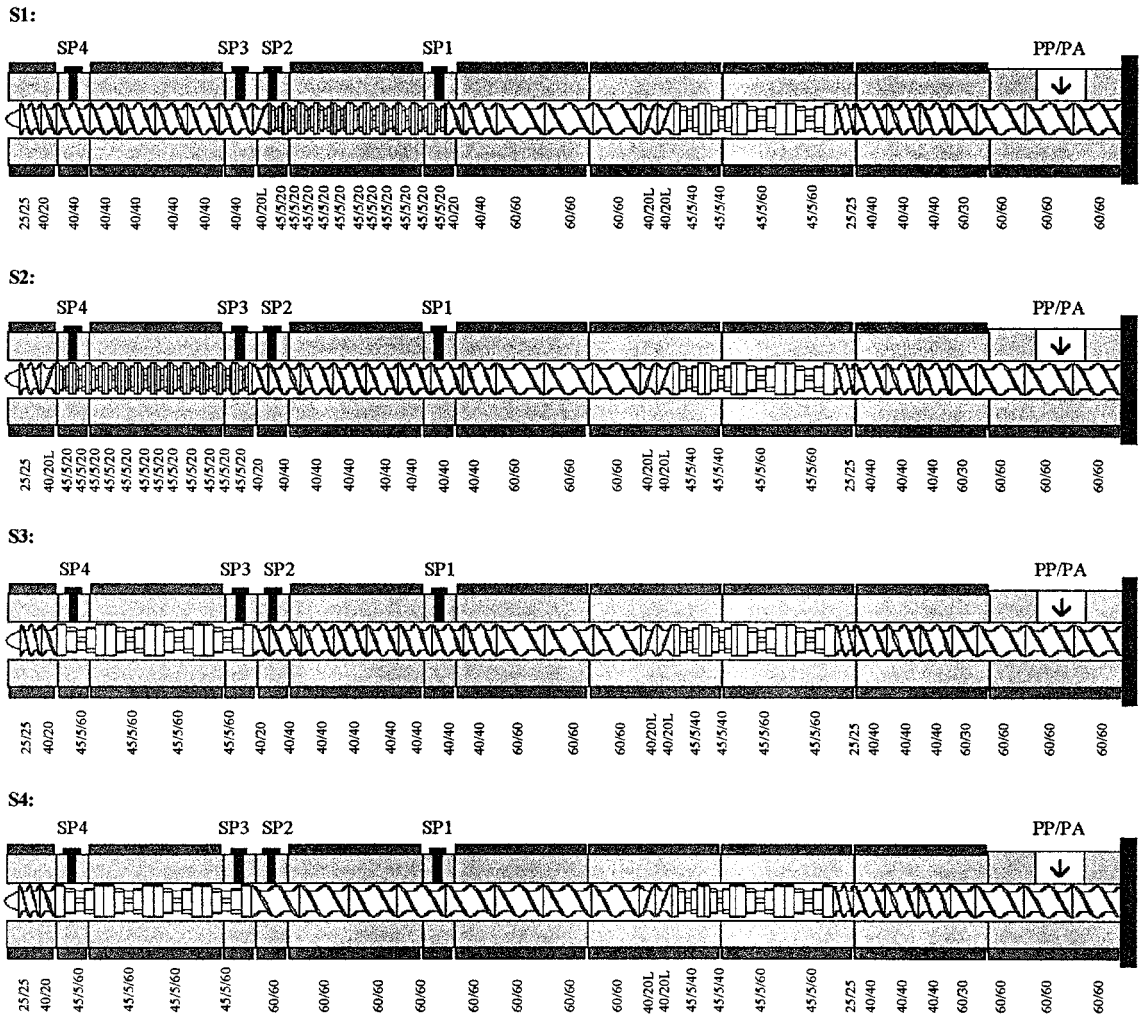

Figure 6 Screw and barrel configurations with sampling points (SPs).

covering a broad geometry spectrum. The total screw and barrel lengths is l_s = 1375 mm for all four screws.

Test Program

Extrusion experiments with the following parameter variations were run:

- screw geometries according to Figure 6,
- mass percentages of dispersed phase (PA) 7.5, 15, 30 wt %,
- total melt throughputs $\dot{m}$ = 35–55 kg/h,
- screw speeds n_s = 100, 150, 200 min^{-1}
- pressures at the screw tips p_D = 1–100 bar as well as
- barrel temperatures T_B = 240–270°C.

Via the die pressure, which could reproducibly be set by means of using a throttle at the die, the back flow length—the length as seen from the tool end of the extruder, until the screw elements are completely filled with material—was set over the measuring range according to the desired process behavior. These settings were easy to monitor and document by means of pressure sensors installed on the sample plates. Table II shows the experiments discussed in this publication including the corresponding extrusion parameters.

Testing and Sampling

Samples were taken during stationary extruder conditions by opening the individual sample plates. From the produced strand, samples of approximately 3 mm in diameter and approximately 5 mm in length were cut out by means of a cut-out tool and immediately cooled down in liquid nitrogen ($T \approx -292$°C), in order to avoid morphology changes. With this quick sampling it was possible

Table II Experiment Overview

No.	Screw	PA [wt %]	Throughput $\dot{m}$ [kg/h]	Screwspeed n_s [min^{-1}]	Pressure ρ_D [bar]	Barrel Temperature T_B [°C]	Melt Temperature T_M [°C]
1	S1	7.5	40	100	90	250	264
2	S1	15	40	100	90	250	Not measured
3	S1	30	40	100	90	250	Not measured
4	S1	7.5	40	100	90	270	274
5	S1	7.5	40	150	90	250	280
6	S1	15	40	150	90	250	Not measured
7	S1	30	40	150	90	250	Not measured
8	S1	7.5	50	150	100	250	270
9	S1	15	55	150	100	250	277
10	S1	30	55	150	100	250	Not measured
11	S1	7.5	50	150	1	250	250
12	S2	7.5	45	100	3	250	246
13	S2	15	50	100	2.5	250	246
14	S3	7.5	40	100	22	250	254
15	S3	15	40	100	15	250	253
16	S4	7.5	45	100	50	250	253
17	S4	15	45	100	50	250	250

to take the sample from the extruder within 5–10 s and to freeze it, thus allowing coalescence processes to be ignored.

Sample Evaluation and Morphology Analysis

For the morphology investigations the samples received from the sample plates were cut by means of a microtome with a glass-cutting knife. The cuts were performed in a cryogenic chamber cooled with liquid nitrogen, below the glass transition temperature of the polymer at $T = -25°C$, in order to prevent the PP matrix from deforming during the cutting. For the quantitative morphology analysis and in order to achieve a good contrast it was necessary to dissolve the dispersed PA6 phase. For this the samples were submerged in 98% formic acid for several hours. The etched samples were then prepared for the investigations with the scanning electron microscopy (SEM). This included the fixation of the samples to special pads and the sputtering of the samples. The cut and etched samples were then morphologically investigated by means of the SEM and an automatic image processing software. A magnification of 1000 was used for all morphologic investigations, which was found to be a magnification in which small particles are visible as well as bigger particles. Figures 7 and 8 show examples of SEMs of the samples. The pictures show that most of the particles are spherical and without adhesion to the matrix.

For the morphology evaluation of the SEM micrographs, in order to determine the particle size, the SEM gray scale image was transformed into a binary image using a brightness threshold setting. The determined area values A_d (the particles touching the frame were not included) are then used to calculate the equivalent circle diameter d.

$$d = \sqrt{\frac{4}{\pi} \cdot A_d}. \tag{3}$$

For further calculations, the so-obtained equivalent diameters are used to calculate the average

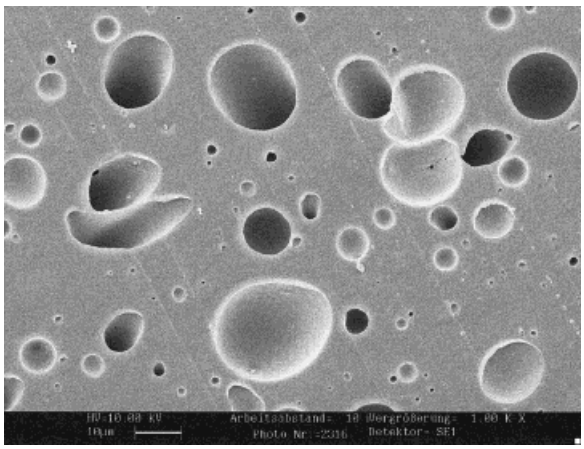

Figure 7 SEM micrograph on a cut and etched sample.

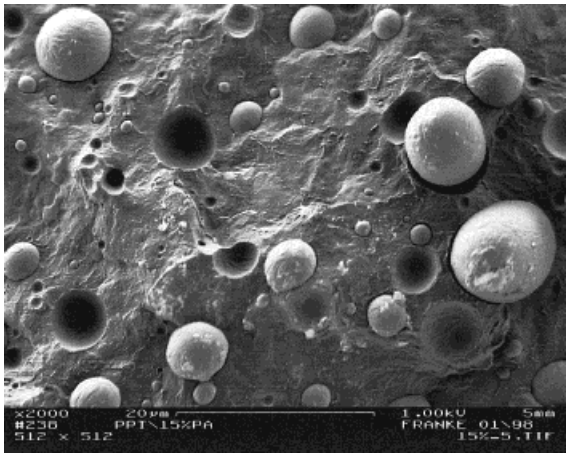

Figure 8 SEM micrograph on a cryo fractured surface.

number (d_n) and the average volume (d_v) diameters:

$$d_n = \frac{\sum_i d_i}{n}, \tag{4}$$

$$d_v = \left(\frac{\sum_i d_i^3}{n} \right)^{1/3}, \tag{5}$$

with n number of particles.

For the determination of the mean particles diameters for each sampling of four samples, 5 SEM micrographs were evaluated (20 SEM micrographs per sampling), so that at least 1100 particles could be counted. It can therefore be assumed that the evaluation of a larger number of particles would not have significantly changed the mean value of particle diameters.[19] For the calculation of the particle size the so-called "tomato slice problem" was neglected. That means, the diameter correction of the particle in the cutting plane, described by Russ[32] for monodispersed, spherical particles, was not performed. Scott[33] and Sundararaj and Macosko[34] found out in the course of their investigations that there is no significant difference between corrected and uncorrected particle size distributions in polydispersed systems. Because bigger particles have a higher probability to touch the frame of the micrographs there is a tendency to neglect them and to obtain a smaller particle size than the blend exhibit. This effect is higher in blends with abroad particle size distribution and big particles. The calculated mean diameters of the evaluated samples are used to quantitatively compare the different test settings and to determine morphologic tendencies.

RESULTS

Influence of the Screw Configuration and the Pressure Profile on the Morphology

The results of the comparison of different screw geometries shows mostly an increase of particle size after passing the re-conveying elements. Figures 9 and 11 show the development of the particle size between the first sample plate and the die, exemplarily for some experiments of screw configuration S1 and 7.5 wt % dispersed phase.

In case of overpassed screw elements and the corresponding backflow caused by the pressure, an increase in coalescence is observed. This can be explained by the increased collision probability of the particles. In case of flow stagnation zone the time of contact between the particles is increased, explaining the coalescence in these fields.

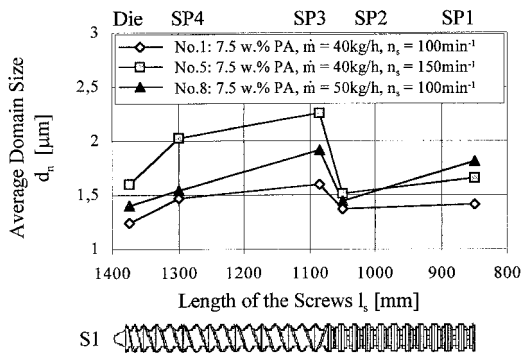

Figure 9 Morphology development for sampling points (SPs) of S1 with 7.5 wt % dispersed phase PA.

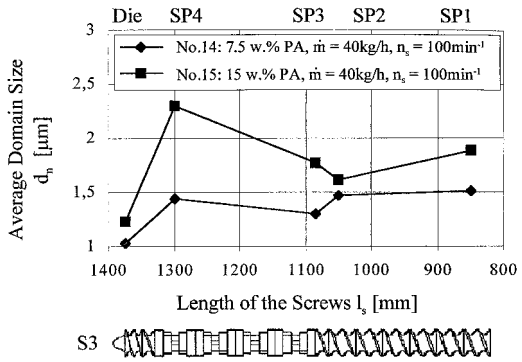

Figure 10 Morphology development in partially filled screw zones for sampling points (SPs) of S3.

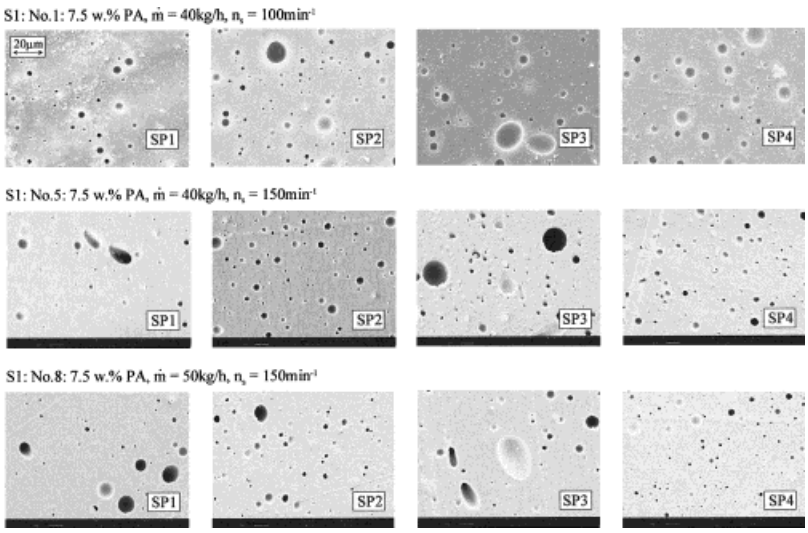

Figure 11 SEM micrographs for sampling points (SPs) of S1 with 7.5 wt % dispersed phase PA.

Mostly partially filled zones show no clear tendencies in the morphology development along the observed melt zones (Fig. 10). After partially filled low-pitch conveying elements, an increase in the mean particle size can be observed in wide kneading elements (KB45/5/60).

The SEMs shown in Figure 11 for the experiments shown in Figure 9 show the existence of a relatively heterogeneous but on average already quite fine morphology after the homogenizing and feed zones. It does not significantly change within the kneading and feed zones of the observed screw section. This observation also applies to zones with a pressure gradient of approximately zero (Figs. 12 and 13). There is insufficient time/shear stress for dispersion and insufficient collision probability for coalescence.

Experiments no. 16 and 17 with screw geometry 4, which has conveying elements of a higher pitch in the first zone as compared with screw 3,

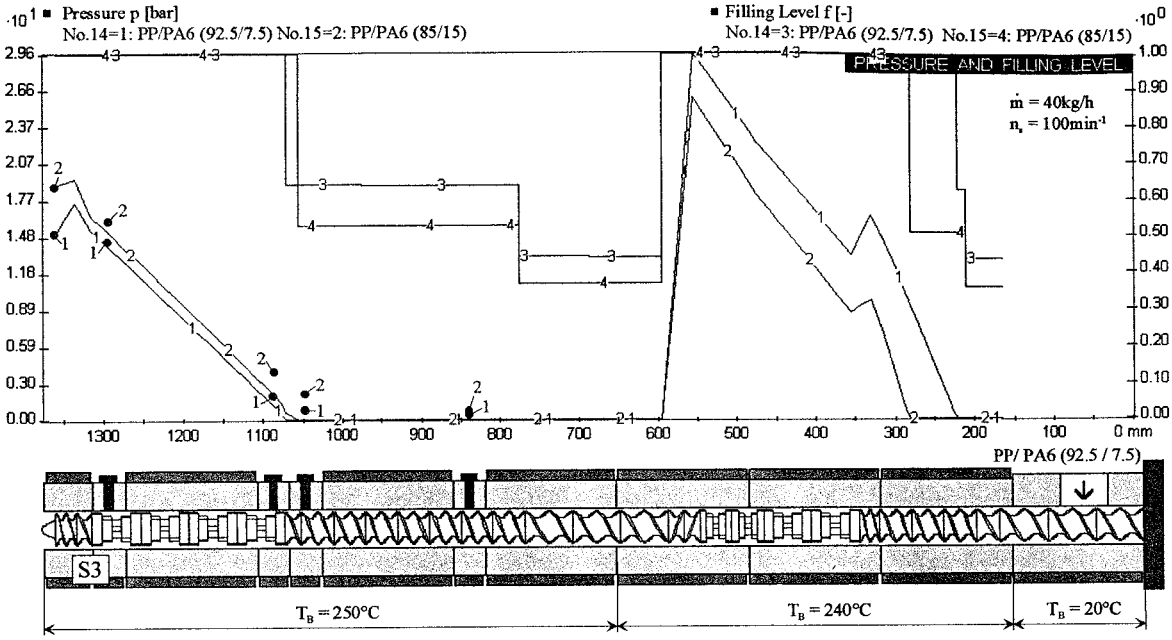

Figure 12 Pressure profile and degree of filling for experiments 14 and 15, measured and calculated with SIGMA.

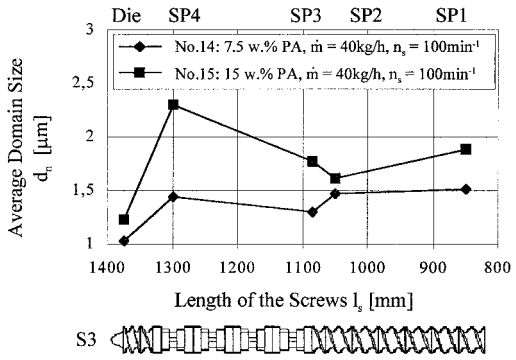

Figure 13 Morphology development for sampling points (SPs) of S3.

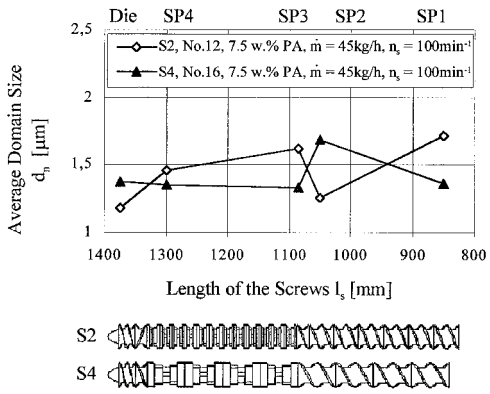

Figure 15 Morphology development for sampling points (SPs) of S2 and S4 with 7.5 wt % dispersed phase PA.

show an increase in particle size in the conveying zone and a reduction or stagnation in the kneading zone (Fig. 14).

Figure 15 also illustrates these facts in a comparison of screw configurations S2 and S4. Evidently, the wider kneading disks seem to have less of a breakup effect than the narrower ones, i.e. the dispersibility does not necessarily increase with wider kneading disks. This observation corresponds to the test results of Franzheim[19] and can be explained by the increase in leakage flows between the individual kneading disks.

Influence of the Content of Dispersed Phase on the Morphology

The experiments with 30 wt % PA always show the largest d_n. The sampling points with 15 wt % PA have medium sized d_n, and the trials with 7.5 wt % PA have the smallest d_n (Figs. 14 and 16). This shows that with an increase in the concentration of the dispersed phase, the mean particle sizes also increases. It is interesting that the degree of changes in morphology caused by the different screw elements is the same for all compositions investigated, which can be explained with an increased coalescence caused by an increasing collision probability in case of a higher number of particles.

Influence of the Rotational Speed on the Morphology

Figures 17 and 18 show the morphology development of experiments with screw S1 with equal melt throughputs and mass percentages of the dispersed phase, but with different rotational speeds.

Figure 17 illustrates, that experiments with 30 wt % dispersed phase PA and the lower rotational speed of 100 min^{-1} achieve smaller particle sizes after the kneading elements as compared with experiments with a rotational speed of 150 min^{-1}. A lower shear rate in connection with a higher residence time, in case of the selected blend system and configuration, consequently results in a finer morphology, analogous to the experimental investigation carried out by Luciani.[35] Figure 18

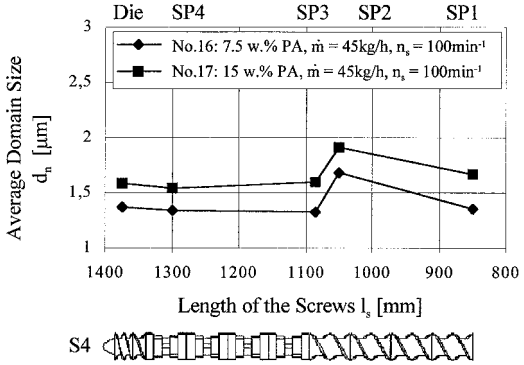

Figure 14 Morphology development for sampling points (SPs) of S4.

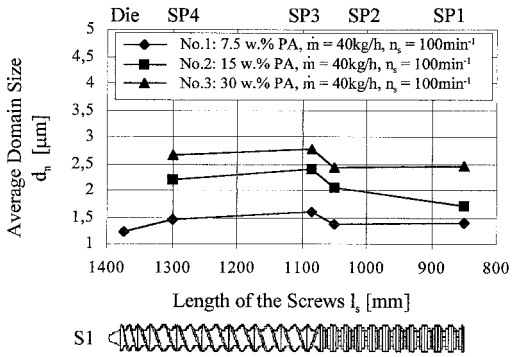

Figure 16 Morphology development for sampling points (SPs) of S1.

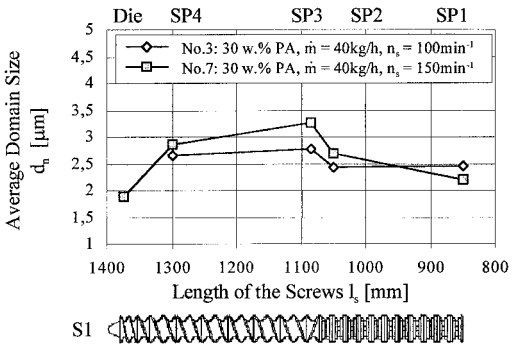

Figure 17 Morphology development of sampling points (SPs) of S1 with 30 wt % dispersed phase PA.

represents the result for 15 wt % dispersed phase. However, it does not show the same tendency of smaller particle sizes in case of lower rotational speeds, as was shown in Figure 17 for 30 wt % dispersed phase.

Thus Figures 17 and 18 show that there is no definite tendency in the relation between morphology development and rotational speed.

Influence of the Melt Throughput on the Morphology

Analogous to the rotational speed, the variation of the melt throughput shows no clear influence on the particle sizes. However, in practice experience shows that a small melt throughput causes higher shear stress and thus higher melt temperatures. This effect, which according to the observations in this study leads to larger particle diameters, does not seem to have had a significant influence on the morphology development in the performed experiments.

Influence of the Temperature on the Morphology

As compared with other sampling points, Figure 19 shows particle sizes above average in the second

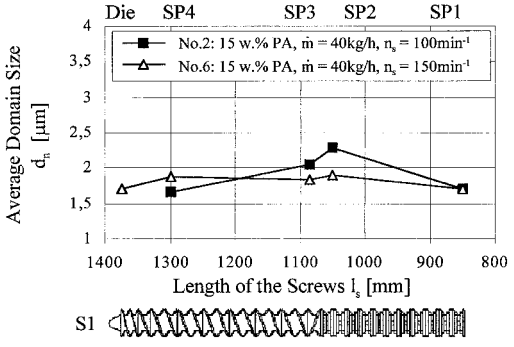

Figure 18 Morphology development of sampling points (SPs) of S1 with 15 wt % dispersed phase PA.

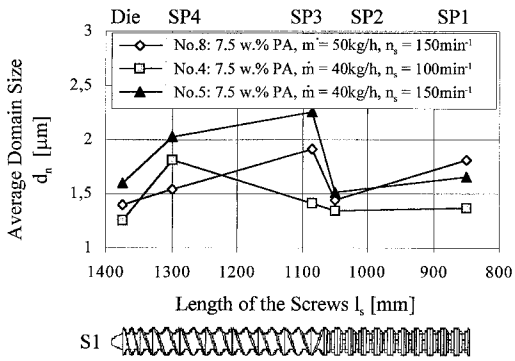

Figure 19 Morphology development for sampling points (SPs) of S1 with 7.5 wt % dispersed phase PA with increasing melt temperature.

measuring zone after the re-conveying element, for Experiments 4, 5, and 8. Experiment 4 also shows a superproportional increase of the d_n between SP3 and SP4. All these show an increased melt temperature in this measuring zone. For this special experiment, the barrel temperature was increased from $T_B = 250°C$ to $T_B = 270°C$. The observed tendency of the particle size development can be explained as follows. The high temperatures lead to a lower viscosity of both components, thus encouraging coalescence because the matrix film between two colliding particles can flow out more easily. The drop breakup on the other hand is more difficult in case of a low matrix viscosity and the consequently dropping capillary number. This effect manifests itself visibly in the particle size developments.

Changes in the Particles Size Distribution

Particularly for higher PA6 concentrations at the beginning of the mixing zones, the direct visual observation of the SEM micrographs show the simultaneous existence of large PA6 particles in the PP matrix (Fig. 20).

Especially in SP1, unmelted PA residues are found in the samples. Downstream, a clear unification of the particle size distribution can be observed (Fig. 20). Particularly the number and size of the coarser particles is decreased in the mixing zones. The courses of melting (Fig. 21), calculated with SIGMA, based on the material characteristics of the mixture shown in Table I show, that at the SP1, particularly for high PA6 concentrations, parts of the mixture are still unmelted, thus explaining the heterogeneous state at the beginning of the mixing zone.

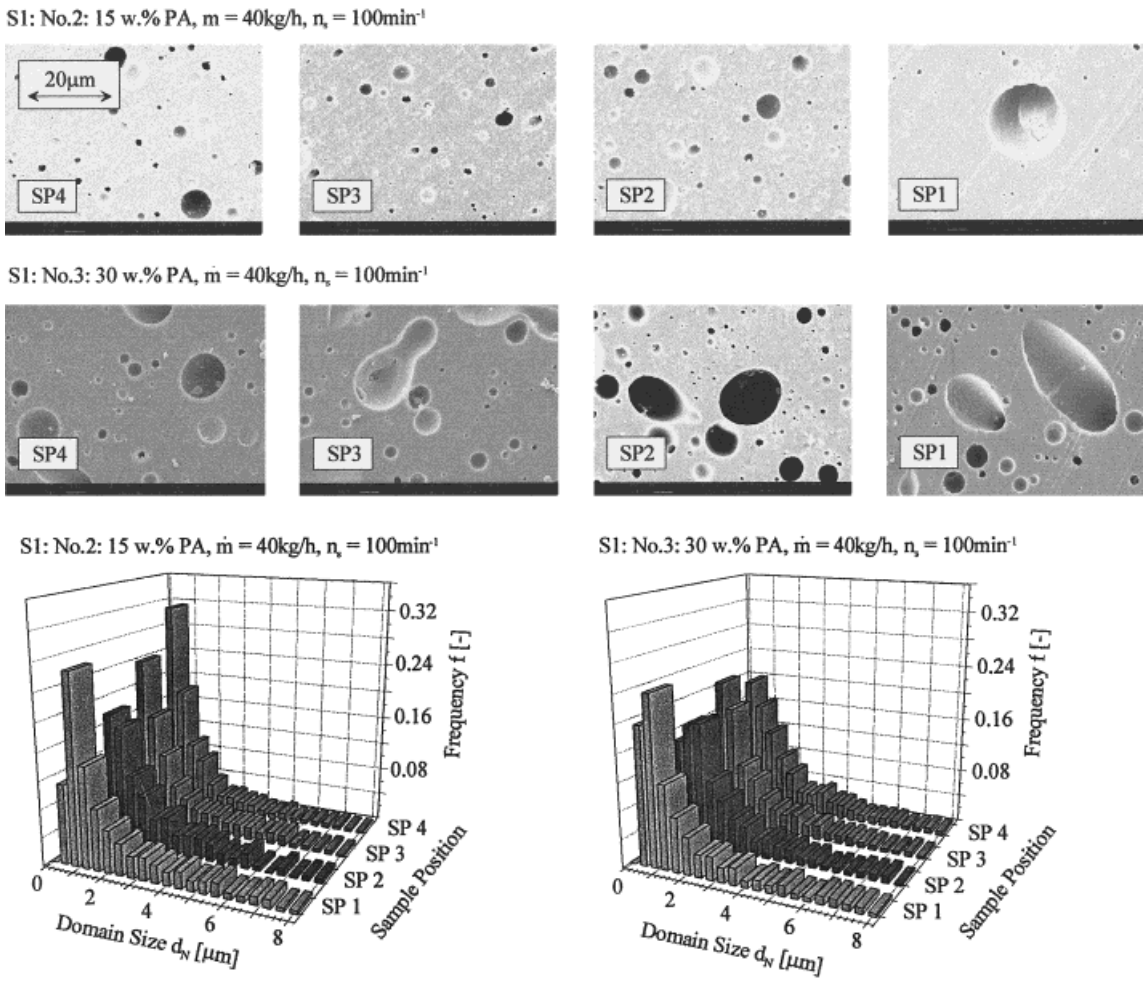

Figure 20 Morphology development for sampling points (SPs) of S1.

SUMMARY AND OUTLOOK

During the experiments, screw geometry, melt throughput, rotational speed, back pressure, and thus backflow length and pressure profiles were changed, and the percentage of the dispersed phase in the blend and the heating zone temperature were varied, in order to examine the different influences of the processing on the morphology development. It is showed that the blend morphologies are very heterogeneous over all measuring zones, and that already at the beginning of the observed zones, the morphology can be very fine, and does not significantly change while passing through the different screw sections, at which samples were taken. For all experiments in the entire measuring range from the beginning of the first measuring zone to the die, the number average particle sizes are between 1.0 to 4.1 μm.

This observation suggests that while flowing through some strong shear and elongation zones inside the extruder, a quasi-final morphology can be achieved, which is for the most part already created in the melting section of the extruder. The observed main effect while passing through the following examined extruder section, is the clear decrease of the width of distribution of the particle sizes, which is well illustrated by the SEMs and which leads to a more even blend morphology.

There are tendencies regarding the influence of the dispersed phase content in the blend, the screw configuration, and the screw speed. An increase in the dispersed phase content results in a coarser morphology with larger particle sizes. In screw sections with re-conveying elements, and in zones with a pressure gradient of practically zero, particle sizes also increase. Depending on the experiment, changing the rotational speed has different influences on the particle size.

Because the major morphologic changes took place prior to the examined mixing zone, further investigations of the morphology development in

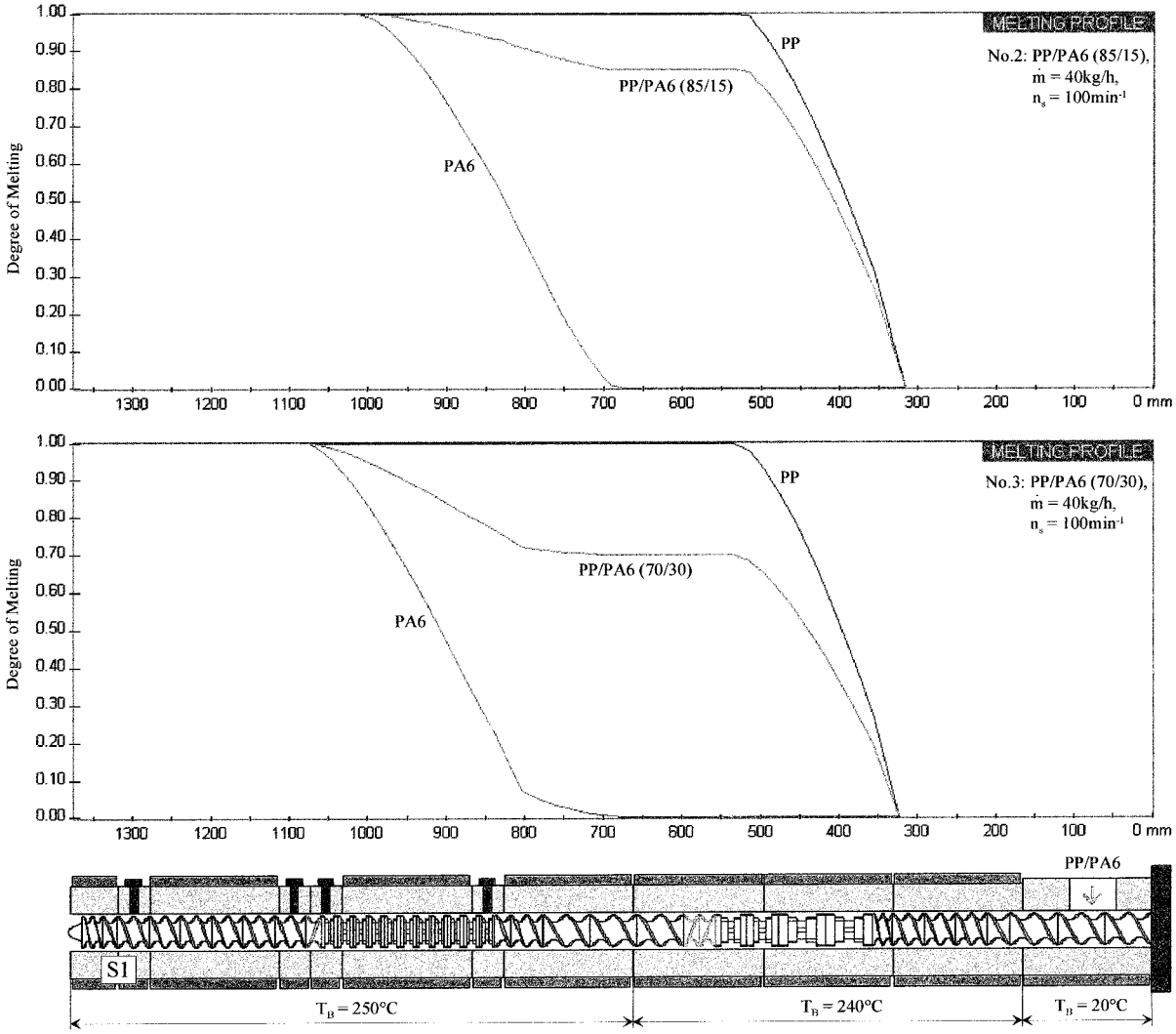

Figure 21 Melting process for sampling points (SPs) of S1, calculated with SIGMA.

the homogenizing section are particularly interesting. Because the main part of the mixing takes place in this section of the extruder, these experiments are also expected to provide starting points for the optimization of this part of the process.

However, because of the special pressure conditions and the high solids content, online sampling in the melting zone is more difficult as compared with SPs where only melt is present.

The realistic assessment of the phase morphology of polymer blends requires a comparative application of different particle analysis and evaluation procedures. The development of effective inline or online analysis methods for the detection of real particle size distributions in representative sample populations will therefore be of particular importance in the future.

The results of this study were achieved in the course of research activities sponsored by the Deutsche Forschungsgemeinschaft (DFG). Special thanks also to BASF AG, Hostalen Polyolefine GmbH, and Krupp Werner & Pfleiderer GmbH for generously providing the materials and test extruder.

SYMBOLS

Roman Symbols

a = Carreau law coefficient
A_d = Area of a domain
b = Carreau law coefficient
c = Carreau law coefficient or specific heat capacity
c_m = Coefficient for the specific heat capacity

c_1 = Williams Landel Ferry (WLF) law coefficient
c_2 = Williams Landel Ferry law coefficient
c_0 = Coefficient for the specific heat capacity
d = Equivalent circle diameter
d_G = Diameter of the granules
d_{Min} = Minimum droplet diameter
d_n = Number average domain size
d_v = Volume average domain size
f = Filling level in screw elements
l_s = Length of the screws
$\dot{m}$ = Throughput
n = Number of domains
n_s = Screw rotational speed
p = Viscosity ratio or pressure
p_D = Pressure at the die
T_B = Barrel temperature
T_K = Melting temperature
T_M = Temperature of the melt at the die
T_R = Reference temperature (WLF-law)
T_S = Standard temperature (WLF-law)
v_0 = Coefficient for the specific volume
v_m = Coefficient for the specific volume
w_c = Weight content of the continuous phase
w_d = Weight content of the dispersed phase

Greek Symbols

Δh = Specific enthalpy
Δh_A = Specific melting enthalpy
Δh_F = Specific solid enthalpy
γ_{12} = Interfacial tension
$\gamma_{12,m}$ = Coefficient for the interfacial tension
$\gamma_{12,o}$ = Coefficient for the interfacial tension
$\dot{\gamma}$ = Shear rate
η = Viscosity
η_c = Viscosity of the continuous phase
η_d = Viscosity of the dispersed phase
η_{Mix} = Viscosity of the polymer blend
ρ_F = Solid density
ρ_S = Bulk density
λ = Flow number or thermal conductivity
λ_O = Coefficient for the thermal conductivity
λ_F = Solid thermal conductivity
λ_m = Coefficient for the thermal conductivity
τ = Shear stress

REFERENCES

1. N/N, Aufbereiten von Polymerblends, 1982, VDI, Düsseldorf.
2. Utracki, L. A. Polymer alloys and blends—Thermodynamics and rheology; Hanser, München, Wien: New York, 1989.
3. Potente, H.; Flecke, J.; Bastian, M. Materiales Poliméricos, Central Català del Plàstic, Sept. 1997, 11.
4. Potente, H.; Flecke, J.; Bastian, M. Adv Polym Techn 1999, 18(2), 147.
5. Potente, H.; Bastian, M. Melting of polymer blends in co-rotating twin screw extruders, Part I: Experimental investigations and models—A review. Intern Polym Proc 1999, submitted.
6. Potente, H.; Flecke, J.; Schramm, D.; Bastian, M. Melting of polymer blends in co-rotating twin screw extruders, Part II: Theoretical derivations. Intern Polym Proc 1999, submitted.
7. Potente, H.; Bastian, M.; Bergemann, M.; Senge, M.; Scheel, G.; Winkelmann, Th. Melting of polymer blends in co-rotating twin screw extruders, Part III: Experimental verification. Intern Polym Proc 1999, submitted.
8. De Loor, A.; Michel, A.; Cassagnau, P.; Vergnes, B. Morphological changes of a polymer blend into a Twin-screw extruder. Intern Polym Proc IX 1994, 3, 211.
9. Taylor, G. I. The formation of emulsions in definable fields of flow. Proc Roy Soc 1934, A146, 501.
10. Bourry, D.; Favis, B. D. Polymer 1998, 39(10), 1851.
11. Favis, B. D. J Appl Polym Sci 1990, 39, 285.
12. Guo-Hua, H.; Cartier, H. Polym Eng Sci 1998, 38(1), 177.
13. Macosko, R. J.; Scott, C. E. Polym Bull 1991, 26, 341.
14. Macosko, C. W.; Sundararaj, U.; Rolando, R. J.; Chan, H. T. Polym Eng Sci 1992, 32(24), 1814.
15. Plochocki, A. P.; Dagli, S. S.; Andrews, R. D. Polym Eng Sci 1990, 30(12), 741.
16. Bordereau, V.; Utracki, L. A.; Shi, Z. H.; Sammut, P.; Carrega, M. Development of polymer blend morphology during compounding in a twin-screw extruder, Part III: Experimental procedure and preliminary results. Polym Eng Sci 1992, 32(24), 1846.
17. Favis, B. D.; Therrien, D. Polymer 1991, 32(8), 1474.
18. Favis, B. D.; Bourry, D. 12th An. Meet. PPS, Sorrento, Italy, 1996, 111.
19. Franzheim, O. Ph.D. Thesis, IPF, Dresden, 1998.
20. White, J. L.; Chen, C. C. Compatibilizing agents in polymer blends: Interfacial tension, phase morphology, and mechanical properties. Polym Eng Sci 1993, 33(14), 923.
21. Wu, S. Phase structure and adhesion in polymer blends: A criterion for rubber toughening. Polymer, 1985, 26, 1855.
22. Pötschke, P.; Wallheinke, K.; Stutz, H. Blends of Thermoplastic Polyurethanes and Maleic-Anhydride Grafted Polyethylene. Polyblends '97 SPE RETEC, International Symposium on Polymer Blends, Alloys and Filled Systems, 1997, 476.
23. Potente, H.; Bastian, M. Polyblends '97 SPE RETEC, International Symposium on Polymer Blends, Alloys and Filled Systems, 1997, 397.

24. Ok Park, O.; Young Moon, D. Adv Polym Techn 1998, 17(3), 203.
25. Patent DE 19531393.3, 1995. Krupp, Werner, & Pfleiderer.
26. Franzheim, O.; Stephan, M.; Rische, T.; Heidemeyer, P.; Burkhardt, U.; Kiani, A. Adv Polym Techn 1997, 16, 1.
27. Schuch, H. Application of a blending rule for the complex viscosity of polymer melts. Rheologica Acta 1988, 27, 384.
28. Utracki, L. A.; Kamal, M. R. Melt rheology of Polymer blends. Polym Eng Sci 1982, 22, 96.
29. Han, C. D.; Kim, Y. W.; Chen, S. J. J Appl Polym Sci 1975, 19, 2831.
30. Plochocki, A. P. Polym Eng Sci 1986, 22, 1153.
31. Potente, H.; Flecke, J. Kunststoffberater, 1997, 5, 14.
32. Russ, J. C. Practical stereology; Plenum Press: New York and London, 1986.
33. Scott, C. E. Characterization of the reactive polymer blending process, Ph.D. Thesis, University of Minnesota, 1990.
34. Sundararaj, U.; Macosko, C. W. Drop breakup and coalescence in polymer blends: The effects of concentration and compatibilization. Macromolecules 1995, 28(8), 2647.
35. Luciani, A.; Champagne, M. F.; Utracki, L. A. Interfacial Tension in Polymer Blends, Part 1: Theory. Polym Networks Blends 1996, 6(1), 41.